Electrochemical behaviour of dysprosium(III) in LiF–CaF_2 on Mo, Ni and Cu electrodes

A. Saïla [a], M. Gibilaro [b], L. Massot [b,*], P. Chamelot [b], P. Taxil [b], A.M. Affoune [a]

[a] *Laboratoire d'Analyses Industrielles et Génie des Matériaux (LAIGM), Université de Guelma, BP 401, Guelma 24000, Algeria*
[b] *Université de Toulouse, INPT, UPS, CNRS; Laboratoire de Génie Chimique, Département Procédés Electrochimiques, F-31062 Toulouse Cedex 9, France*

A B S T R A C T

The electrochemical behaviour of dysprosium(III) was investigated in the LiF–CaF_2 eutectic mixture on molybdenum, nickel and copper electrodes in the 840–930 °C temperature range using cyclic voltammetry, square wave voltammetry and chronopotentiometry. On Mo electrode, the study showed that Dy(III) ions were reduced into Dy metal in a one-step diffusion-controlled process exchanging three electrons: $Dy(III) + 3e^- \leftrightarrow Dy$. The diffusion coefficients verify the Arrhenius law, allowing the activation energy to be calculated. The study of the electrochemical reduction of Dy(III) ions on reactive electrodes (Ni, Cu) first by cyclic voltammetry showed that the reduction potential of Dy(III)/Dy on reactive electrodes was observed at more positive values than those on inert electrode and then open-circuit chronopotentiometry put into evidence the formation of intermetallic compounds at more anodic potentials than pure dysprosium. Preparation of alloys layers was finally carried out by intentiostatic electrolyses at underpotential compared to the pure metal deposition; SEM observations of the layer allowed the most stable compounds prepared by this way to be identified.

1. Introduction

Partitioning and Transmutation (P&T) of long-lived fission products and minor actinides are considered as one of the future options for nuclear waste management. Up to now, nuclear industries consider mainly hydrometallurgical methods such as the PUREX process for spent fuel treatment [1]. An alternative route should be the use of "dry" pyrochemical separation methods in non aqueous solvents. The separation processes by electrodeposition from molten salts appear to be acknowledged in all networks based on the nuclear of future. Compared with aqueous solvents, the choice of molten salts, such as alkali fluorides, is based on their relevant solvent properties. For electrochemical applications: larger electrochemical window, higher electrodeposition rates and better characteristics of the deposits [2,3]. Thanks to these advantages, pyrochemical reprocessing becomes more important for the implementation of the P&T programs to decrease the amount and long-term hazards of nuclear wastes.

In the frame of research works realized in our laboratory for establishing appropriate conditions to separate actinides (An) from lanthanides (Ln) and other fission products (FP) [4–7] in molten fluorides media, we plane to investigate on the intrinsic electrochemical parameters of all the elements concerned in order to obtain the background data relevant for the future An–Ln separation and extraction process in these media. In particular we observed that, in most cases, the Ln elements cannot be extracted completely from the solvent as pure metals on an inert electrode, because their equilibrium potential is too closed from the solvent wall, whereas we obtained almost 100% for the extraction rate of Nd and Gd on a reactive electrode where the metal is yielded in alloyed form [8].

In the present article, we study the electrochemical behaviour of dysprosium (which is one of the Ln produced in nuclear reactors) in DyF_3–LiF–CaF_2 for examining the possibilities of extraction from nuclear wastes either in pure state or alloyed one with a reactive cathode. A variety literature is available relating to the dysprosium in molten salts and often reports results of electro reduction of Dy(III) both on inert and reactive cathodes. Besides, the electro reduction pathway is controversial, about whether the intermediate Dy(II) participates or not to the electrode process. However the most noticeable contribution concerns the study of the reduction mechanism of Dy(III) ions by Castrillejo et al. [9] where the authors found a two-steps reduction mechanism in LiCl–KCl–$DyCl_3$ system in the 400–550 °C temperature range on W electrode as:

$$Dy(III) + 1e^- \leftrightarrow Dy(II) \quad (1)$$

$$Dy(II) + 2e^- \leftrightarrow Dy(0) \quad (2)$$

* Corresponding author. Tel.: +33 5 61 55 81 94; fax: +33 5 61 55 61 39.
E-mail address: massot@chimie.ups-tlse.fr (L. Massot).

The authors also investigate the formation of $DyAl_3$ alloy using potentiostatic electrolysis on aluminium reactive electrode.

Elsewhere, Chang et al. [10] proposed, in the same chloride medium, an electrochemical reduction in a one-step process exchanging three electrons, in agreement with Konishi et al. [11–14] who measured, in the same system at 500 °C, a reduction potential of 0.47 V vs. Li^+/Li Ref. [11]. Furthermore, they have evaluated, on Fe and Ni electrodes, the equilibrium potential of Fe–Dy and Ni–Dy compounds and calculated their thermodynamic properties. Always in chlorides salts, a spectroscopic study of some trivalent lanthanides, carried out by Fujii et al. [16], evidenced the dependence of the $DyCl_6^{3-}$ complex geometry on temperature and nature of the salts. Zeng et al. [15] performed a similar study in $Li2CO_3^-$ K_2CO_3 mixture at 377 °C on Ni electrode.

The separation of FP by phosphate precipitation in molten chlorides was studied by Volkovich et al. [17] in the 550–750 °C temperature range. The effect of the PO_4^{3-} ions addition on the distribution coefficient of Dy(III) and other fission products has been examined.

The purpose of the present article is to determine the electrochemical behaviour of $LiF–CaF_2–DyF_3$ system on different substrates: (i) inert electrode (Mo) in order to study the electrodeposition of Dy metal, (ii) reactive electrodes (Ni, Cu) for the formation of intermetallic compounds. The experimental techniques used were cyclic voltammetry, square wave voltammetry, chronopotentiometry and open-circuit chronopotentiometry.

2. Experimental

The cell consisted of a vitreous carbon crucible placed in a cylindrical vessel made of refractory steel and closed by a stainless steel lid cooled by circulating water. The inner part of the cell walls was protected against fluoride vapours by a graphite liner. The experiments were performed under an argon (less than 5 ppm O_2) atmosphere, previously dehydrated and deoxygenated using a purification cartridge (Air Liquide). The cell was heated using a programmable furnace and the temperatures were measured using a chromel–alumel thermocouple.

The electrolytic bath consisted of a eutectic $LiF–CaF_2$ (Merck 99.99%) mixture (79/21 M ratio). Before use, it was dehydrated by heating under vacuum (10^{-2} mbar) from ambient temperature up to its melting point (762 °C) for 48 h. Dysprosium ions were introduced into the bath in the form of pellets of dysprosium trifluoride, DyF_3 (Merck 99.99%).

Electrodes: molybdenum wire (1 mm diameter) was used as inert working electrode, nickel (1 mm diameter) and copper wires (1.2 mm diameter) were used as reactive electrodes. The area of the working electrode was determined after each experiment by measuring the immersion depth in the bath. The auxiliary electrode was a vitreous carbon (V25) rod (3 mm diameter) with a large surface area (2.5 cm^2). The potentials were referred to a platinum wire (0.5 mm diameter) immersed in the molten electrolyte, acting as a quasi-reference electrode $Pt/PtO_x/O^{2-}$ (QRE) with a potential remaining constant for a given low oxide content in the bath [18].

The electrochemical techniques used to the study of the electroreduction process of Dy(III) species (cyclic voltammetry, square wave voltammetry and chronopotentiometry), were performed with an Autolab PGSTAT 30 potentiostat/galvanostat controlled by computer using the GPES 4.9 software.

The cathode surface areas were examined after electrochemical reduction by Scanning Electron Microscopy (LEO 435 VP) with EDS probe (Oxford INCA 2000).

3. Results and discussion

3.1. DyF_3 electrochemical reduction mechanism on inert electrode

First, the dysprosium E-pO^{2-} diagram, plotted in Fig. 1 from HSC 5.1 software at 840 °C (1113 K) with all soluble species activities equal to 0.1 mol kg^{-1}, allows dealing with the following inquiries:

– For low oxide contents, only DyF_3 and Dy are observed. So, DyF_2 is not considered as thermodynamically stable; this result is in agreement with those obtained by Bratsch et al. [19]. According to this diagram, DyF_3 should be electrochemically reduced into Dy, so the only predicted reaction is:

$$DyF_3 + 3e^- \leftrightarrow Dy + 3F^- \quad (3)$$

This reaction occurs at lower cathodic potential than the solvent discharge ($Li^+ + e \leftrightarrow Li$). Consequently, Dy metal deposition was considered theoretically possible on inert electrode.

– At high O^{2-} ions activity ($pO^{2-} < 2.8$), DyF_3 precipitates into Dy_2O_3 stable oxide. So, to avoid its formation, the free oxide content in the bath must be kept at low values.

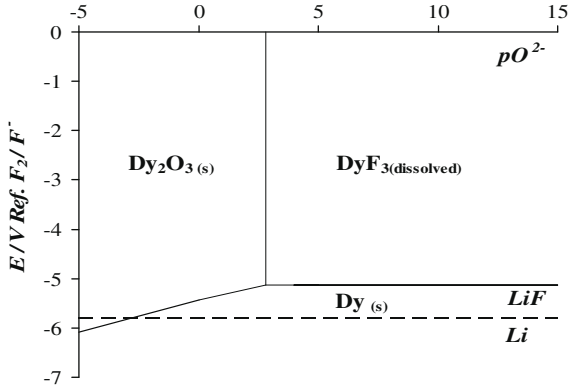

Fig. 1. E-pO^{2-} diagram made using HSC 5.1 software at 840 °C in the $LiF–sCaF_2$ melt and all soluble species activities equal to 0.1 mol kg^{-1}.

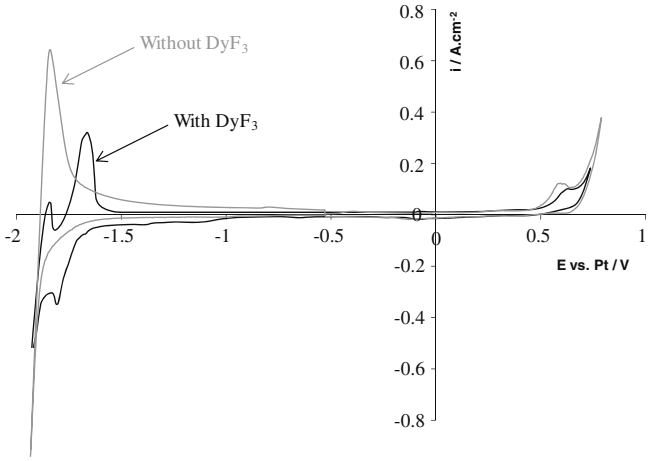

Fig. 2. Typical cyclic voltammogram of $LiF–CaF_2–DyF_3$ (9.4×10^{-5} mol cm^{-3}) system, compared with the one of $LiF–CaF_2$ at 100 mV s^{-1} and 840 °C. Working El.: Mo (S = 0.4 cm^2); auxiliary El.: vitreous carbon; quasi-reference El.: Pt.

3.1.1. Cyclic voltammetry

Cyclic voltammetry was carried out on inert Mo electrode in the 840–930 °C temperature range. Fig. 2 shows a typical voltammogram obtained for LiF–CaF_2–DyF_3 (9.4×10^{-5} mol cm^{-3}) system, compared with the one of the pure solvent. This voltammogram exhibits one reduction peak (I_c) at −1.76 V vs. Pt, just prior to solvent reduction wave (Li^+/Li).

Notice that prior to the reduction peak I_c, a sensitive cathodic current wave which is independent on the Dy(III) content, and thereby attributed to an adsorption process. Comparing this voltammogram with the one of the pure solvent (grey plotting) evidences that the reduction wave of Dy(III) interferes with the Li^+ reduction, so that the current peaks of Dy(III) must be measured after withdrawing the solvent current and adsorption wave.

In the anodic part, the shape of the associated reoxidation peak (I_a) is typical of a stripping phenomenon, indicating that the cathodic product is a metallic phase.

Fig. 3 demonstrates the linear relationship between the cathodic peak current density and the DyF_3 concentration. Consequently, the cathodic peak should be attributed to Dy(III) reduction into Dy(0). Subsequently, the investigation of the potential scan rate influence on the peak current density was performed. Fig. 4 shows the linear relationship between the reduction peak intensity and the square root of the scan rate, proving that the electrochemical reduction process is controlled by the Dy(III) ions diffusion in the solution. The current density was correlated to the potential scan rate with the adequate Berzins–Delahay equation [20]:

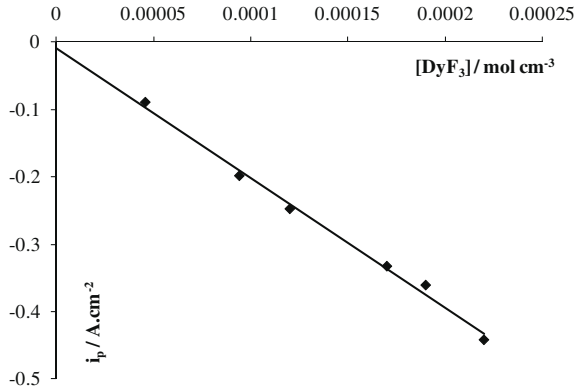

Fig. 3. Linear relationship between the DyF_3 cathodic peak current density (100 mV s^{-1}) and the DyF_3 concentration in the melt at 840 °C.

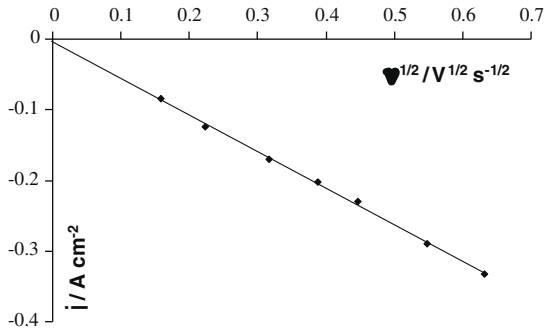

Fig. 4. Linear relationship between DyF_3 electroreduction peak density and the square root of the potential scan rate at $T = 840$ °C and $C = 9.4 \times 10^{-5}$ mol cm^{-3}. Working El.: Mo ($S = 0.283$ cm^2); auxiliary El.: vitreous carbon; quasi-reference El.: Pt.

$$I_p = -0.61nFSC\left(\frac{nF}{RT}\right)^{1/2} D^{1/2}\nu^{1/2} \quad (4)$$

where n is the number of exchanged electrons, F is the Faraday constant (C mol^{-1}), S is the surface area (cm^2), C is the solute concentration (mol cm^{-3}), T is the absolute temperature (K), D is the diffusion coefficient (cm^2 s^{-1}), R is the gas constant (J mol^{-1} K^{-1}) and ν is the potential scan rate (V s^{-1}).

From the results of Fig. 4, the slope of the straight line has been measured, for $T = 870$ °C and $C = 9.4.10^{-5}$ mol cm^{-3}:

$$\frac{I_p}{\nu^{1/2}} = -0.52 \pm 0.02 \text{ A s}^{1/2} \text{ V}^{-1/2} \text{ cm}^{-2} \quad (5)$$

Other values of this slope for various temperatures are reported in Table 1.

Combination of Eqs. (4) and (5) can be used to calculate the diffusion coefficients.

3.1.2. Chronopotentiometry

In order to confirm the diffusion-control of the reduction process, several chronopotentiograms were plotted on Mo electrode (see Fig. 5). These curves show a single plateau at around −1.75 V vs. Pt, corresponding to the reduction of Dy(III) into Dy. It can be observed that the transition time (τ) decreases with the increase of the applied current density. Fig. 6 reports the relationship between $i\tau^{1/2}$ and the applied current density, in agreement with the Sand's law:

$$i\tau^{1/2} = -0.5nFCD^{1/2}\pi^{1/2} = \text{constant} \quad (6)$$

This equation was verified at different temperatures. The results from Fig. 6 give, for $T = 870$ °C and $C = 2.94 \times 10^{-4}$ mol cm^{-3}:

$$i\tau^{1/2} = -0.49 \pm 0.01 \text{ A s}^{1/2} \text{ cm}^{-2} \quad (7)$$

The chronopotentiometric analysis confirmed the diffusion-control of the Dy(III) ions reduction process.

3.1.3. Determination of the number of exchanged electrons

Using square wave voltammetry, it was possible to determine the number of exchanged electrons, in order to confirm Eq. (3). This method was detailed in previous work [21]. For a single reversible process, the current–potential curve is a Gaussian peak symmetrically axed on a potential close to the half-wave potential and with the peak height proportional to the concentration of the electroactive species. Besides, the half-width, $W_{1/2}$, depends on the number of exchanged electrons and on the temperature as follow [22]:

$$W_{1/2} = 3.52\frac{RT}{nF} \quad (8)$$

Fig. 7 presents a typical square wave voltammogram of the LiF–CaF_2–DyF_3 system on Mo electrode at $f = 9$ Hz and $T = 840$ °C. It exhibits a symmetrical single peak at −1.86 V vs. Pt. As explained in previous works [23,24], the linearity of the current peak density with the square root of the frequency assumes the reversibility of the process which allows applying the last equation. This relationship has been verified in the 9–70 Hz

Table 1
Slopes values of Berzins–Delahaye relation and diffusion coefficient values of DyF_3 in different temperature for the concentration 9.4×10^{-5} mol cm^{-3} of DyF_3.

T (K)	1113	1143	1173	1203
C (mol cm^{-3})	9.4×10^{-5}			
S (cm^2)	0.28	0.30	0.28	0.31
$I_p/\nu^{1/2}$ (A s$^{1/2}$ V$^{-1/2}$ cm^{-2})	−0.52	−0.59	−0.66	−0.74
10^5 D (cm^2 s^{-1})	3.10 ± 0.03	4.18 ± 0.06	5.37 ± 0.04	6.95 ± 0.04

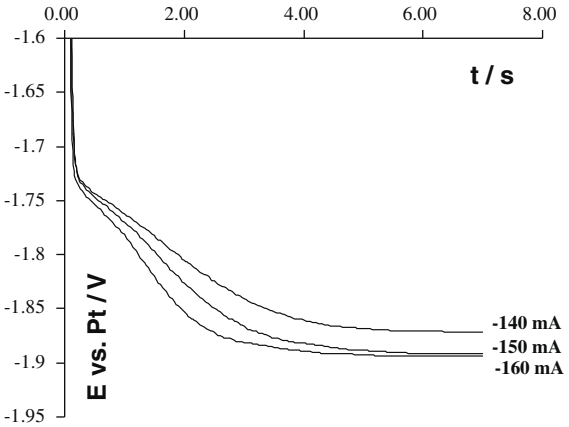

Fig. 5. Typical chronopotentiograms with the applied current density of LiF–CaF_2–DyF_3 (2.94×10^{-4} mol cm^{-3}) system at 840 °C. Working El.: Mo ($S = 0.392$ cm^2); auxiliary El.: vitreous carbon; quasi-reference El.: Pt.

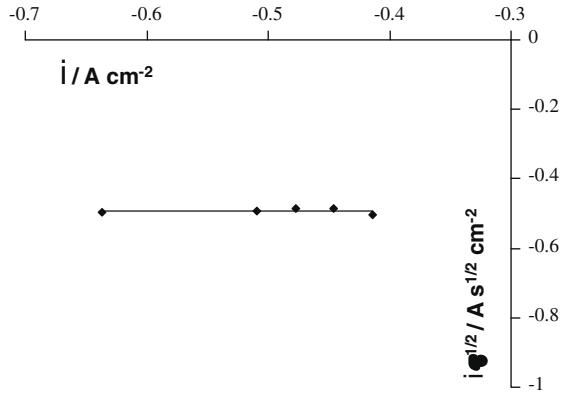

Fig. 6. Linear relationship between $i\tau^{1/2}$ and the applied current density. $T = 840$ °C and $C = 2.97 \times 10^{-4}$ mol cm^{-3}. Working El.: Mo ($S = 0.392$ cm^2); auxiliary El.: vitreous carbon; quasi-reference El.: Pt.

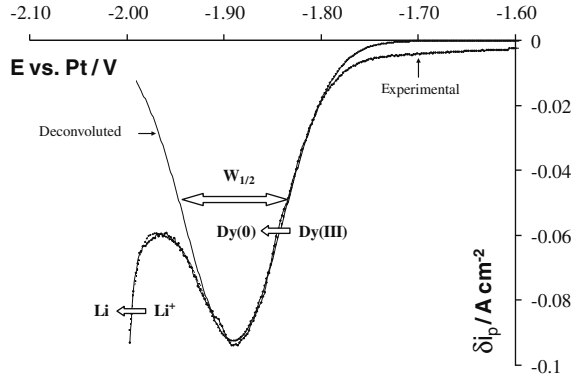

Fig. 7. Typical square wave voltammogram of the LiF–CaF_2–DyF_3 (9.4×10^{-5} mol cm^{-3}) system at frequency $f = 9$ Hz and $T = 840$ °C. Working El.: Mo ($S = 0.314$ cm^2); auxiliary El.: vitreous carbon; quasi-reference El.: Pt.

frequency range. The deconvolution of the experimental curve reveals one peak corresponding to the reduction of Dy(III) ions. By measuring the half-width of this peak, the number of exchanged electrons has been calculated, using Eq. (8): $n = 3.0 \pm 0.1$. This result lets us conclude that the electrochemical reduction of Dy(III) into Dy(0) on inert electrode is a one-step process exchanging three electrons:

$$DY(III) + 3e^- \leftrightarrow Dy(0) \tag{9}$$

3.1.4. Diffusion coefficient of Dy(III) ions

Dy(III) diffusion coefficients have been calculated using voltammetric results using Eq. (4) and experimental data with $n = 3$ at different temperatures. The results are gathered in Table 1.

The variation of ln(D) vs. the inverse of the absolute temperature has been plotted in Fig. 8. The linear relationship observed proves that the diffusion coefficient variation with T obeys an Arrhenius law:

$$D = D^0 \exp\left(-\frac{E_a}{\mathrm{RT}}\right) \tag{10}$$

where E_a is the activation energy in J mol^{-1}, T is the absolute temperature in K, D is the diffusion coefficient in cm^2 s^{-1}. The results from Fig. 8 give the following equation:

$$\ln D = 0.348(\pm 0.002) - \frac{11937(\pm 60)}{T} \tag{11}$$

From this equation the activation energy is found to be -99.2 ± 0.5 kJ mol^{-1}.

3.1.5. Extraction of dysprosium on inert cathode

According to Fig. 2, the difference between the equilibrium potential of Dy ions in the molten fluorides and the solvent potential wall can be evaluated at about 100 mV, whereas in Fig. 1 this difference is sensibly larger, that can be explained by calculation of the limits of the stability domains are calculated with pure solid species; with Nernst equation in this temperature range, we estimate than 290 mV are required to get a theoretical extraction efficiency of 99.99% [25]. Taking into account this calculation, only around 96% of Dy extraction from the molten salt can be expected.

3.2. Electroreduction of Dy(III) ions on Ni and Cu reactive electrodes: formation of intermetallic compounds

Dysprosium can form alloys with more noble metals such as nickel and copper. As reported in the phase diagrams of Dy–Ni and Dy–Cu [26], different intermetallic compounds exist for these metals: (i) ten for Dy–Ni system (Dy_3Ni, Dy_3Ni_2, DyNi, $DyNi_2$, $DyNi_3$, Dy_2Ni_7, $DyNi_4$, Dy_4Ni_{17}, $DyNi_5$, and Dy_2Ni_7), (ii) six for Dy–Cu system (DyCu, $DyCu_2$, Dy_2Cu_7, Dy_2Cu_9, $DyCu_5$ and $DyCu_7$).

The feasibility of alloying process of the electroactive species with the cathode substrate was commonly studied by electrochemical techniques [8,27–30]. Likewise here, the analysis of the electrodeposition on reactive substrates and the characterization of the formed intermetallic compounds were carried out by cyclic voltammetry and open-circuit chronopotentiometry.

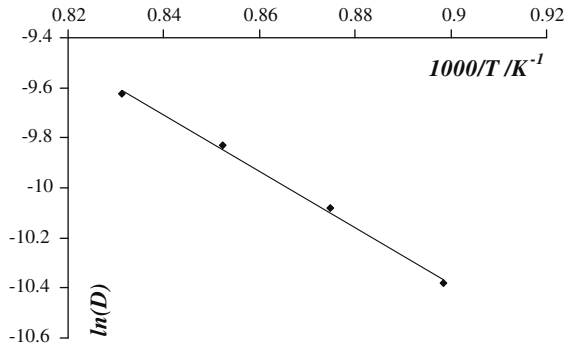

Fig. 8. Linear relationship between the logarithm of DyF_3 diffusion coefficient and the inverse of the absolute temperature.

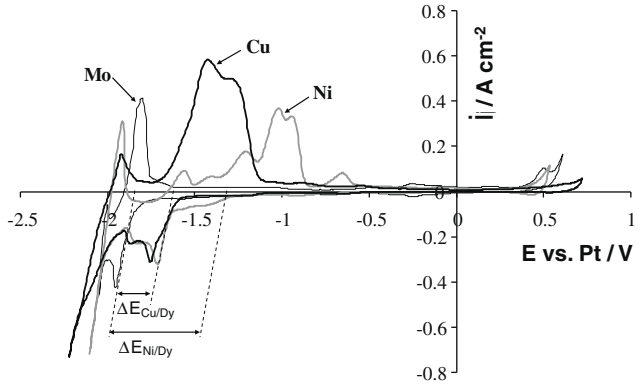

Fig. 9. Comparison of cyclic voltammograms of LiF–CaF_2–DyF_3 (9.4×10^{-5} mol cm^{-3}) system on molybdenum, nickel and copper electrodes at 100 mV s^{-1} and T = 840 °C. Auxiliary El.: vitreous carbon; quasi-reference El.: Pt.

3.2.1. Cyclic voltammetry

Fig. 9 compares cyclic voltammograms of LiF–CaF_2–DyF_3 system plotted at 100 mV s^{-1} and 840 °C on molybdenum inert electrode with (a) nickel and (b) copper. The plots on Ni and Cu are very different from the one on Mo. Besides the peak at −1.86 V vs. Pt, corresponding to the reduction of Dy(III) into Dy metal on Mo, higher reduction currents are observed on the curves plotted on Ni and Cu. These currents are placed in a large potential range prior the reduction of pure metal: −1.35 to −1.86 V vs. Pt for Ni and −1.6 to −1.86 V vs. Pt for Cu system. Of evidence, these currents can be attributed to the formation of Dy–Ni and Dy–Cu of the respective binary phase diagrams.

If we refer to Section 3.1.5, the shift of the discharge potential of Dy ions on reactive electrode lets to expect now 100% extraction of Dy from the molten salt.

3.2.2. Open-circuit chronopotentiometry

Open-circuit chronopotentiometry is a suitable technique to investigate the formation of intermetallic compounds of Ln–Ni and Ln–Cu systems and to calculate their Gibbs free energies [8,26–30]. The methodology was: first, Ln element is deposited on the Ni or Cu reactive electrodes using short intentiostatic electrolysis; then the polarization was stopped and the electrode was kept in the molten salt. During this currentless step, where only intermetallic diffusion occurs, the open-circuit potential was recorded vs. time; meanwhile the electrode potential was shifted towards more positive values following successive plateaus. A potential plateau is observed when the composition of the electrode surface is shared between two intermetallic compounds. When a two-phase equilibrium at the surface of the electrode occurs, the dysprosium activity is the same in each phase and remains constant while the overall Ln concentration at the surface decreases.

Figs. 10a and 10b show, for Ln = Dy, a typical open-circuit chronopotentiogram recorded after cathodic polarization of DyF_3 on Ni and Cu electrodes at 870 °C. During this process, eleven plateaus were observed for Ni electrode and seven for Cu electrode. The first plateau corresponds to the equilibrium potential of Dy deposited at −1.81 V vs. Pt for Ni and −1.80 V vs. Pt for Cu. The successive plateaus, related to the different compounds of the Dy–Ni and Dy–Cu phase diagrams, start from the intermetallic compound with the richest Dy content to the one with the lowest content. Each potential plateau is referred to the standard potential of the Dy that makes it possible to determine the electromotive force (emf) of the cell Dy_xM/Dy_yM/LiF–CaF_2–DyF_3/Dy, which is associated to the reaction:

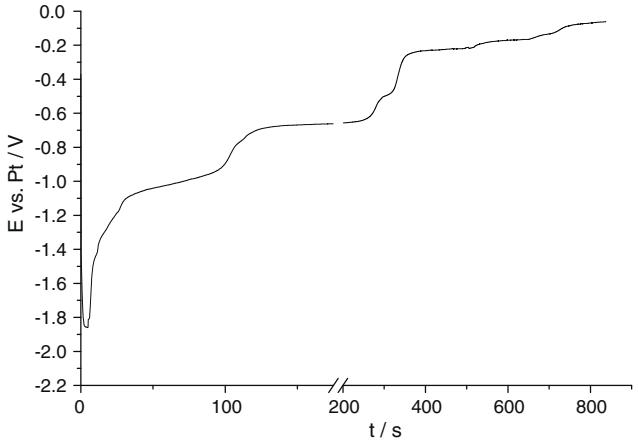

Fig. 10a. Open-circuit chronopotentiograms of LiF–CaF_2–DyF_3 (9.4×10^{-5} mol cm^{-3}) system on nickel electrode at T = 840 °C. Auxiliary El.: vitreous carbon; quasi-reference El.: Pt.

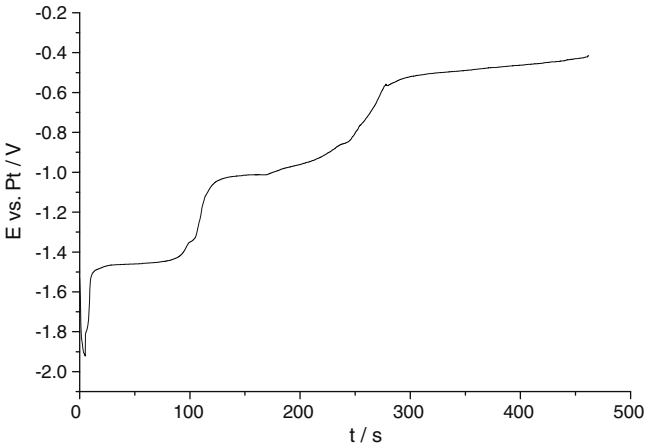

Fig. 10b. Open-circuit chronopotentiograms of LiF–CaF_2–DyF_3 (9.4×10^{-5} mol cm^{-3}) system on copper electrode at T = 840 °C. Auxiliary El.: vitreous carbon; quasi-reference El.: Pt.

$$Dy_xM + (y - x)Dy + (m - 1)M \leftrightarrow Dy_yM_m \quad (12)$$

After the first plateau, the next one corresponds to the formation of the first intermetallic compound with the highest content of Dy in the binary phase diagrams: Dy_3Ni and DyCu for Dy–Ni and Dy–Cu systems respectively.

The potential of each plateau referred to the one of pure Dy in Figs. 10a and 10b is the e.m.f. associated to Eq. (12).

Such e.m.f. measurements allowed us to calculate the thermodynamic properties of Ln alloys with Cu and Ni, as mentioned above, but in the present work, the too high number of potential plateaus and, correlatively, of intermetallic compounds in the binary diagram, made too difficult for us to obtain accurate similar results with Dy compounds.

Nevertheless, Figs. 10a and 10b allow evaluating the successive potentials of formation of each compound of the binary diagrams Dy–Cu and Dy–Ni; as Ni and Cu are more noble elements than Dy, the potential of these plateaus is assumed to be increasing (in the cathodic sense) with the Dy content in the binary compound.

3.2.3. Formation of Dy–Ni and Dy–Cu surface alloys

The previous paragraph lets us to predict that dysprosium can be extracted from the molten salts in an alloyed form at electrolysis performed within the potential range defined as ΔE in fig. 9,

thus at underpotential compared with the pure Dy deposition. For extracting Dy by underpotential electrodeposition, potentiostatic or intensiostatic modes can be employed; according to a discussion about this subject in a previous paper, concerning another system [31], we can assume that:

- Potentiostatic electrolysis at the most anodic potentials within ΔE yields low content compounds in Dy; at higher potentials (up to the potential of pure Dy deposition) one obtains several compounds of the binary diagram in the alloy surface layer, further to the intermetallic diffusion.
- Intensiostatic electrolysis, with a cathodic potential control leads to a mixture of compounds in the alloy layer. This method can be preferred because it is the most rapid.
- Coherent layers containing the most stable compounds can be obtained by keeping the cathodic sample in the molten salts after electrolysis [27,31].

In order to investigate the Dy–Ni and Dy–Cu intermetallic compounds formation, several intentiostatic electrolyses were carried out at different current densities and durations on Ni and Cu electrodes. Afterwards, the cross sections of the samples were observed by Scanning Electron Microscopy (SEM) and their composition determined. Typical SEM micrographs are presented in Fig. 11 and Fig. 12 for Ni and Cu respectively. The variation of the current density and the electrolysis time has a great influence on the alloys composition. The following remarks can be noted:

- In each system, whatever the current, the Dy content is decreasing in the surface alloy layer towards the substrate, that confirms the intermetallic diffusion effect and that the stability scale of these compounds is an inverse function of the Dy content.
- At lower currents and long electrolysis durations, only poorest in Dy compounds (Dy_2Ni_{17}, $DyNi_4$; $DyCu_5$, $DyCu_5$, $DyCu_4$) are observed, that should mean that the intermetallic diffusion rate is higher than the electrochemical reaction at the surface cathode, which yields the richest in Dy compounds. At high currents and durations, the layer includes also compounds with higher Dy contents, almost at the electrolyte interface ($DyNi_2$ and $DyNi_3$; $DyCu_2$); as a rule, the highest content and the lower one are pointed out at the electrolyte and the substrate interface respectively.
- Partial detachment of the electrodeposited layer can be observed on each micrography, typical of the Kirkendal effect, which is relevant of a difference of diffusion rate between the

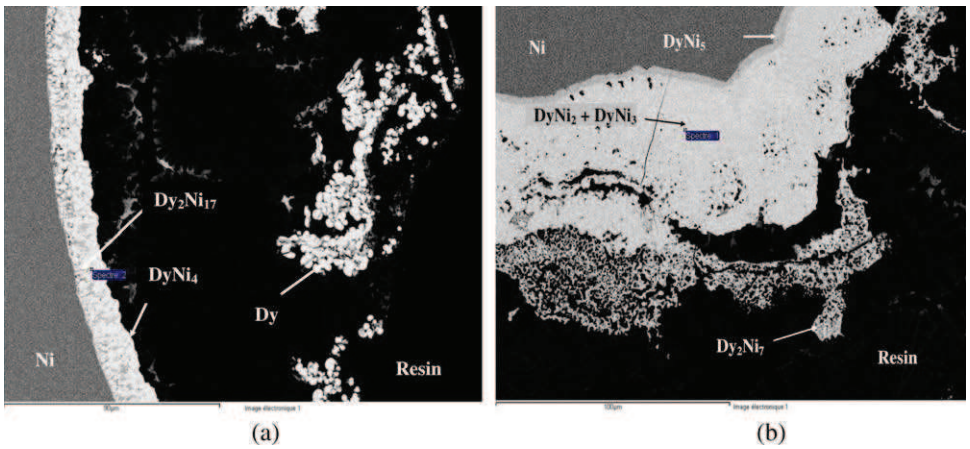

Fig. 11. Different SEM micrographs of the cross section of nickel electrodes after electroreduction of DyF_3: (a) at T = 840 °C; i = −15 mA cm^{-2}; t = 3600 s and (b) at T = 870 °C; i = −150 mA cm^{-2}; t = 1200 s.

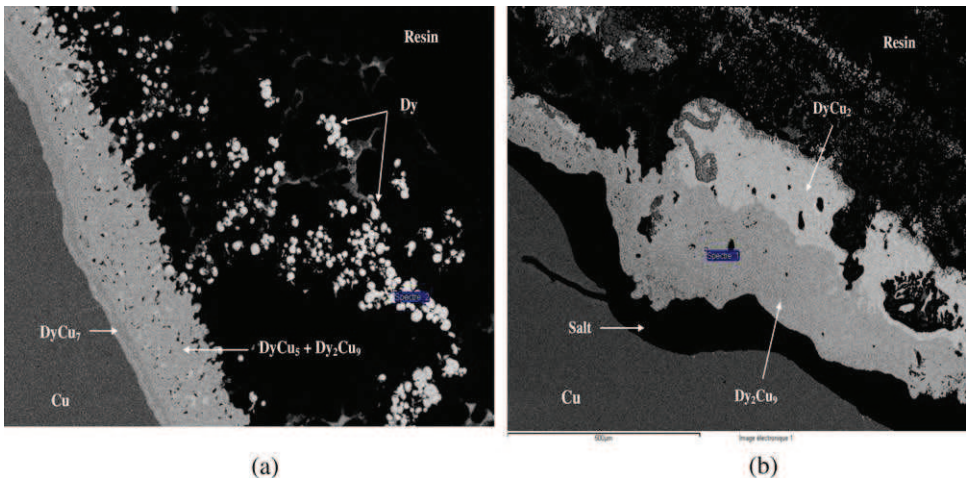

Fig. 12. Different SEM micrographs of the cross section of copper electrodes after electroreduction of DyF_3: (a) at T = 840 °C; i = −16 mA cm^{-2}; t = 3600 s and (b) At T = 870 °C; i = −120 mA cm^{-2}; t = 1200 s.

species: at low currents, this effect promotes the release of pure Dy metal in the bath whereas at higher currents, the whole alloy layer is expelled from the substrate.

One can conclude from these observations that dysprosium can be extracted easily from the molten solution in the form of pure metal or alloy.

The comments above are in agreement with other systems studied in our laboratory: Nd, Gd/Ni, Cu by Nourry et al. [8,32] and Al/Ni by Gibilaro et al. [31].

The use of reactive cathodic substrates, like Ni or Cu, offers a potential depolarization allowing high extraction rates of dysprosium from molten fluoride baths to be expected. This kind of process confirms the pertinent choice of reactive substrate in the extraction operations.

4. Conclusion

The study of the electrochemical reduction of dysprosium in the $LiF–CaF_2$ eutectic mixture was performed on molybdenum (inert), nickel and copper (reactive) electrodes. The results of the electrochemical analysis on Mo show that the reduction mechanism of Dy(III) occurs in a one-step process exchanging three electrons as:

$$Dy(III) + 3e^- \leftrightarrow Dy(0)$$

In addition, the results on Mo demonstrate that this process is controlled by the Dy(III) diffusion in the solution. The Dy(III) ions diffusion coefficients were calculated from cyclic voltammetry measurements and showed a temperature dependence in agreement with the Arrhenius law.

The cyclic voltammetry and open-circuit chronopotentiometry studies, on reactive electrodes, proved that dysprosium can be reduced by alloying the cathodic substrate. The open-circuit chronopotentiograms allow associating the potential plateaus with certain of the compounds mentioned in the phase diagrams. Investigations by SEM with EDS probe of the interdiffusion layer makes it possible to identify these intermetallic compounds for each system.

The whole results of this work allow stating that the complete extraction of dysprosium from a molten solution providing from nuclear wastes is possible by electrochemical way, but only by underpotential electrodeposition on a reactive cathode.

References

[1] CEA, Report PG-DRRV/DIR/00-92, Assessment of Pyrochemical Processes for Separation and Transmutation Strategies-proposed Areas of Research, 2000.
[2] P. Taxil, P. Chamelot, L. Massot, C. Hamel, J. Min. Metall. 39 (1–2) (2003) 177–200.
[3] R.S. Sethi, J. Appl. Electrochem. 9 (1979) 411–426.
[4] L. Massot, P. Chamelot, P. Taxil, Electrochim. Acta 50 (2005) 5510–5517.
[5] C. Hamel, P. Chamelot, A. Laplace, E. Walle, O. Dugne, P. Taxil, Electrochim. Acta 52 (2007) 3995–4003.
[6] P. Chamelot, L. Massot, C. Hamel, C. Nourry, P. Taxil, J. Nucl. Mater. 360 (2007) 64–74.
[7] C. Nourry, L. Massot, P. Chamelot, P. Taxil, Electrochim. Acta 53 (2008) 2650–2655.
[8] C. Nourry, L. Massot, P. Chamelot, P. Taxil, J. Appl. Electrochem. 39 (2009) 2359–2367.
[9] Y. Castrillejo, M.R. Bermejo, A.I. Barrado, R. Pardo, E. Barrado, A.M. Martínez, Electrochim. Acta 50 (2005) 2047–2057.
[10] K.G. Chang, X.P. Ping Lu, Y.Y. Du, M.S. Zhao, Chinese J. Chem. 12 (1994) 509–516.
[11] H. Konishi, T. Nohira, Y. Ito, Electrochim. Acta 47 (2002) 3533–3539.
[12] H. Konishi, T. Nohira, Y. Ito, Electrochim. Acta 48 (2003) 563–568.
[13] H. Konishi, T. Nohira, Y. Ito, Electrochim. Acta 48 (2003) 1403–1408.
[14] H. Konishi, T. Nohira, Y. Ito, J. Electrochem. Soc. 148 (7) (2001) C506–C511.
[15] C.L. Zeng, T. Zhang, P.Y. Guo, W.T. Wu, Corros. Sci. 46 (2004) 2183–2189.
[16] T. Fujii, T. Nagai, A. Uehara, H. Yamana, J. Alloys Compd. 441 (2007) L10–L17.
[17] V.A. Volkovich, T.R. Griffiths, R.C. Thied, J. Nucl. Mater. 323 (2003) 49–56.
[18] A.D. Graves, D. Inman, Nature 208 (1965) 481–482.
[19] S. Bratsch, H.B. Silbert, Polyhedron 1 (3) (1982) 219–223.
[20] T. Berzins, P. Delahay, J. Am. Chem. Soc. 75 (1953) 555–571.
[21] J.G. Osteryoung, J.J. O'Dea, Electroanal. Chem. 14 (1986) 209–220.
[22] L. Ramaley, M.S. Krause, Anal. Chem. 41 (1969) 1362–1370.
[23] P. Chamelot, B. Lafage, P. Taxil, Electrochim. Acta 39 (1994) 2571–2575.
[24] P. Chamelot, B. Lafage, P. Taxil, Electrochim. Acta 43 (1997) 607–616.
[25] P. Taxil, L. Massot, C. Nourry, M. Gibilaro, P. Chamelot, L. Cassayre, J. Fluorine Chem. 130 (2009) 94–101.
[26] Binary Alloys Phase Diagrams, second ed., ASM international, 1996.
[27] P. Taxil, J. Less-common Met. 113 (1985) 89–101.
[28] F. Lantelme, J. Chevalet, J. Electroanal. Chem. 121 (1981) 311–327.
[29] G.S. Picard, Y.E. Mottot, B.L. Trémillon, Proceedings of the Fourth International Symposium on Molten Salt, vol. 84(2), Electrochem. Soc., 1984.
[30] Y. Ito, Proceedings of the International Symposium on Molten Salt and Technology, vol. 93, Electrochem. Soc., 1993.
[31] M. Gibilaro, L. Massot, P. Chamelot, P. Taxil, J. Alloys Compd. 471 (2009) 412–420.
[32] C. Nourry, L. Massot, P. Chamelot, P. Taxil, J. New Mater. Electrochem. Syst. 10 (2007) 117–122.